Article

Stretchable Self-healing Polymeric Dielectrics Crosslinked Through Metal-Ligand Coordination

Ying-Li Rao, Alex Chortos, Raphael Pfattner, Franziska Lissel, Yu-Cheng Chiu, Vivian Feig, Jie Xu, Tadanori Kurosawa, Xiaodan Gu, Chao Wang, Mingqian He, Jong Won Chung, and Zhenan Bao

J. Am. Chem. Soc., **Just Accepted Manuscript** • DOI: 10.1021/jacs.6b02428 • Publication Date (Web): 21 Apr 2016

Stretchable Self-healing Polymeric Dielectrics Crosslinked Through Metal-Ligand Coordination

Ying-Li Rao,[a] Alex Chortos,[b] Raphael Pfattner,[a] Franziska Lissel,[a] Yu-Cheng Chiu,[a] Vivian Feig,[b] Jie Xu,[a] Tadanori Kurosawa,[a] Xiaodan Gu,[a] Chao Wang[a], Mingqian He,[c] Jong Won Chung,[a,d] Zhenan Bao[a,]*

[a]Department of Chemical Engineering, [b]Materials Science and Engineering Department, Stanford University, California, 94305, USA
[c]Corning Incorporated, SP-FR-06-1, Corning, NY 14831, USA
[d]Samsung Advanced Institute of Technology Yeongtong-gu , Suwon-si, Gyeonggi-do 443-803 , South Korea
**Corresponding Author: zbao@stanford.edu*

Abstract

A self-healing dielectric elastomer is achieved by the incorporation of metal-ligand coordination as crosslinking sites in non-polar polydimethylsiloxane (PDMS) polymers. The ligand is 2,2'-bipyridine-5,5'-dicarboxylic amide while the metal salts investigated here are Fe^{2+} and Zn^{2+} with various counter anions. The kinetically labile coordination between Zn^{2+} and bipyridine endows the polymer fast self-healing ability at ambient condition. When integrated into organic field-effect transistors (OFETs) as gate dielectrics, transistors with $FeCl_2$ and $ZnCl_2$ salts crosslinked PDMS exhibited increased dielectric constants compared to PDMS and demonstrated hysteresis-free transfer characteristics, owing to the low ion conductivity in PDMS and the strong columbic interaction between metal cations and the small Cl^- anions which can prevent mobile anions drifting under gate bias. Fully stretchable transistors with $FeCl_2$-PDMS dielectrics were fabricated and exhibited ideal transfer characteristics. The gate leakage current remained low even after 1000 cycles at 100% strain. The mechanical robustness and stable electrical performance proved its suitability for applications in stretchable electronics. On the other hand, transistors with gate dielectrics containing large-sized anions (BF_4^-, ClO_4^-, $CF_3SO_3^-$) displayed prominent hysteresis

due to mobile anions drifting under gate bias voltage. This work provides insights on future design of self-healing stretchable dielectric materials based on metal-ligand crosslinked polymers.

1. Introduction

Flexible electronics have generated tremendous interest among scientific and engineering community.[1–5] Due to their light weight, flexibility, large-area printability[6], and potential biodegradability[7,8], organic based flexible electronics hold great potential in applications such as wearable electronics[9] and medical devices[10]. Moreover, the ability to self-heal upon rupture or scratch can significantly improve the devices' lifetime. Various strategies have been applied to achieve organic self-healable conductors[11], luminescent materials[12], and battery electrodes[13].

However, self-healing electronic materials still remain limited. For repeatable autonomous self-healing materials, the ability to restore their original mechanical properties upon damage relies on the incorporation of dynamic molecular bonds, namely stimuli-induced reversible bond breaking and reformation[14]. Dynamic molecular bonds are divided into two general categories: covalent adaptive bonds, or supramolecular noncovalent bonds, such as hydrogen bonding, π-π stacking, hydrophobic, host-guest complexation, metal-ligand coordination. Compared to other dynamic molecular bonds, metal-ligand coordination interactions are particularly attractive, as a broad range of molecular parameters, such as the identity of the metal ions, counter ions, and ligands can be varied to tune the bond strengths, endowing desirable material properties. A wide selection of dynamic metal-ligand interactions has been exploited in the literature for the development of self-healable materials. For example, Bielawski *et al* showed a class of thermally healable organometallic conducting polymers comprising group 10 transition metal salts (Ni, Pd and Pt) and N-heterocyclic carbenes[15]. Rowan, Weder and coworkers reported photo-activated healable supramolecular polymers employing coordination between La^{3+}, Zn^{2+} metal ions and 2,6-bis(1-methylbenzimidazolyl)pyridine[16]. Holten-Andersen and coworkers prepared a self-healing gel containing Fe^{3+}-catechol coordinate bonds[17]. Guan *et al* developed a hard/soft two-phase brush copolymer integrating Zn^{2+}-imidazole interactions in the soft matrix, which exhibited autonomous self-healing ability at room temperature[18]. Our group has recently reported a concept to achieve materials with ultra-stretchability and self-healing ability through embedding dual-strength

dynamic metal-ligand coordination bonds within the soft PDMS polymer backbone[19]. The concept of "dual-strength dynamic bonds" refers to that in the deprotonated 2,6-dicarboxylic amide pyridine (PDCA) chelating ligand, the coordination geometry around Fe^{3+} metal center is stabilized by the strong coordination through central pyridyl nitrogen along with the flanking either amide oxygen or amide nitrogen anion.

While significant progress has been made in the area of self-healing materials using metal-ligand coordination, applications of materials containing metal-ligand coordination for self-healable electronics remain largely unexplored. Considering that transistors are the basic elements in integrated circuits, we have been developing various strategies for stretchable and self-healable materials for various components in organic field-effect transistors (OFETs). One advantage of introducing metal-ligand coordination bonds into dielectric is that their high polarizability can potentially increase the dielectric constant, which is a desirable feature for gate dielectric materials to reduce operating voltage. While there are few recent reports about self-healing insulating dielectrics for OEFTs, they are either based on inorganic metal oxide[20] which are incompatible with low-cost printing fabrication methods, or ion-polarized dielectric materials that suffer significant drop of capacitance along with the increase of applied electric field frequency[21]. Here we describe a new self-healing polymer system, which employs metal-ligand (Fe^{2+}, Zn^{2+}-bipyridine) interactions. To our knowledge, this is the first example of integrating such a system into organic field-effect transistors as gate insulators. Furthermore, we demonstrate that the transistor electrical stability is closely related to the size of the counter anions of metal ion cross-linkers.

2. Results and Discussion

2.1 Materials Design and Synthesis

Bipyridine moiety is one of the most widely used neutral ligands in literature, owing to its well-defined coordination geometry with a variety of transition metal ions[22]. It has been utilized to construct molecular knots[23,24], metal-organic frameworks (MOF)[25], or the directed self-assembly of peptides[26]. As shown in Fig. 1a, our design strategy is to embed bipyridine moieties into a long

polydimethylsiloxane(PDMS) chain, which is subsequently crosslinked via metal-ligand coordination between bipyridine moieties and transition metal ions, Zn^{2+} and Fe^{2+}. While the inherent low T_g of PDMS endows the polymer chains ample motion freedom at room temperature, the choice of metal salts gives us an additional knob to tune the crosslink density and polymer dynamics. The non-polar PDMS matrix is also important for dielectric application as it reduces ion mobility and ionic effects that may be caused by intentional incorporation of ions. The coordination between the bidentate ligand bipyridine and Fe^{2+} is typically octahedral geometry[27], with the bond length of N(bipyridyl)-Fe^{2+} being around 1.97 Å[28]. In contrast, Zn^{2+} ions with $3d^{10}$ outer shell electrons, which don't have the ligand-field stabilization effects, show a high degree of flexibility to adopt either tetrahedral or octahedral geometry[29], depending on the counter anions, solution concentration and temperature[30]. In an octahedral geometry, the bond length between N(bipyridyl) and Zn^{2+} is around 2.15 Å[31], which is significantly longer than that of N(bipyridyl)-Fe^{2+}, suggesting that the coordination bond between N(bipyridyl) and Zn^{2+} is more kinetically labile. Moreover, the dynamic coordinating ability of counter anions can help stabilize the complex structure and could potentially serve as energy dissipation sites in bulk materials[32]. Anions with coordinate strength in the order of chloride (Cl^-) >> triflate (OTf: $CF_3SO_3^-$) > tetrafluoroborate (BF_4^-), perchlorate(ClO_4^-) are investigated here.

Bipyridine moieties were incorporated into the PDMS backbone via the equal molar condensation reaction between bis-amine terminated PDMS with 2,2'-bipyridine 5,5'-dicarboxylic acid chloride. Addition of 0.33 eq of metal salts in the form of $FeCl_2$, $Fe(BF_4)_2$, $ZnCl_2$, $Zn(OTf)_2$ or $Zn(ClO_4)_2$ into the solution of bpy-PDMS (~ 1eq bipyridine moieties) all caused solution gelation, which indicated the metals salt served as effective cross-linkers (Fig. 2e). UV-Vis absorption spectroscopy was used to monitor metal ion binding stoichiometry (Fig. 2a-c). The well-defined isosbestic points in all the UV-Vis absorption spectra indicate clean, stoichiometric coordination between bipyridine and Fe^{2+} or Zn^{2+} metal ions. Regardless of the counter anions (Cl^-, BF_4^-), the addition of Fe^{2+} salts to bpy-PDMS solution all generated a magenta solution with a maximum

absorbance at 558 nm, characteristics of the metal-to-ligand charge transfer electronic transition. The absorption spectra reached saturation in a relative molar ratio of 1:3 Fe^{2+}: bpy-PDMS, consistent with the literature reported octahedral geometry between Fe^{2+} and bidentate ligand bipyridine[33]. In the case of Zn^{2+} salts, the different counter anions have distinct impacts on the coordination geometry. During the titration experiments, the initial addition of Zn^{2+} salts ($ZnCl_2$, $Zn(ClO_4)_2$, $Zn(OTf)_2$) all resulted in a similar change of the UV-Vis absorption spectra, with a bathochromic shift of the bipyridine ligand-centered π-π* electronic transition. With continuous addition of $Zn(ClO_4)_2$ or $Zn(OTf)_2$ up to ~0.33 : 1 ratio to bipyridine moieties, the UV-Vis absorption spectra reached saturation, which denotes the 1:3 (metal:ligand) octahedral coordination geometry between Zn^{2+} and bipyridine moieties. In the case of $ZnCl_2$, due to the strong coordinating ability of Cl^-, in the reported small molecule models, the coordination geometry between $ZnCl_2$ and bipyridine is generally tetrahedral at room temperature with the two chloride anions tightly bound to the Zn^{2+} center[34], and 1:3 (metal:ligand) octahedral geometry at elevated temperature. However, upon addition of $ZnCl_2$ to bpy-PDMS solution, the viscosity change implied the crosslinks among polymer chains. The similarities of changes in the UV-Vis spectra upon the initial addition of Zn^{2+} salts ($ZnCl_2$, $Zn(ClO_4)_2$, $Zn(OTf)_2$) also suggested the 1:3 coordination geometry between $ZnCl_2$ and bipyridine moieties. The surprising octahedral coordination geometry between $ZnCl_2$ and bipyridine moieties at room temperature indicates a low reaction activation barrier in the polymer system. The isosbestic points slightly shifted after 0.2 eq addition of $ZnCl_2$, suggesting the appearance of ordinary tetrahedral coordination geometry (Fig. 2d). Thus, the binding geometry in $ZnCl_2$-PDMS is a combination of an initial ~60% 1:3 octahedral geometry with ~40% non-crosslinked tetrahedral coordination (Fig. 1b). The distinct coordination geometries are reflected in the polymers' mechanical properties and self-healing ability.

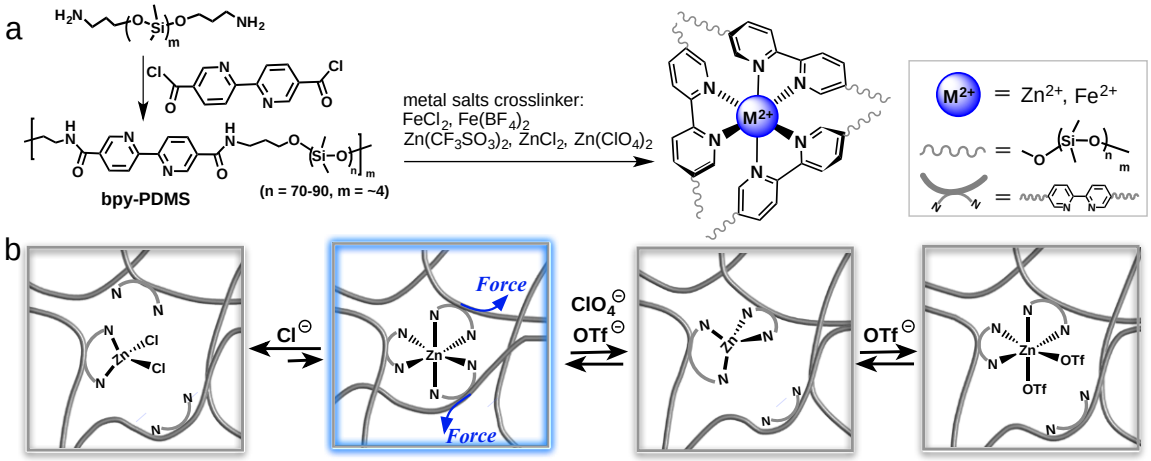

Figure 1 (**a**) The synthetic route of metal salts crosslinked PDMS. (**b**) Schematic illustrating the proposed dynamic interactions among metal cations Zn^{2+}, the ligand and the counter anions in the polymer systems under mechanical stress.

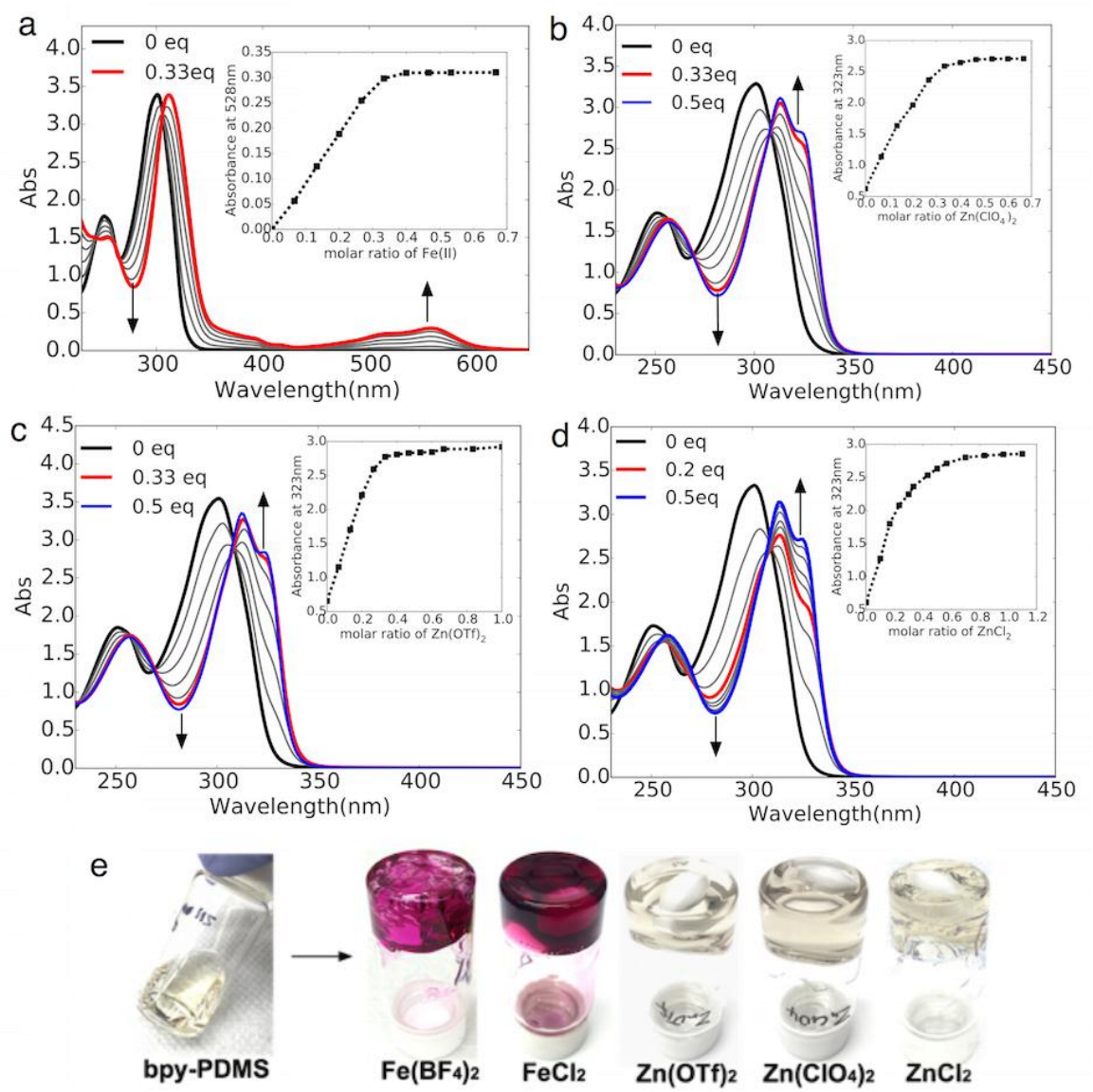

Figure 2 UV-Vis absorption spectra acquired upon titration of bpy-PDMS (1×10^{-4} M bipyridine moieties) in CH_2Cl_2 with $FeCl_2$ (**a**), $Zn(ClO_4)_2$ (**b**), $Zn(OTf)_2$ (**c**) and $ZnCl_2$ (**d**), respectively. The inset in (**a**) shows the absorption at 528nm as a function of Fe^{2+}:bpy-PDMS. The insets in (**b**), (**c**), (**d**) show the absorption at 323 nm as a function of Zn^{2+}:bipyridine moieties. (The interval between each addition is 0.066 eq.) (**e**) Images showing the gelation formations of **bpy-PDMS** toluene solution (70 mg/ml, 3 ml) upon the addition of methanol solution of the various metal salts crosslinker (0.18 M/L, 50 μl).

2.2 Mechanical Properties

Polymer films were prepared by solution cast into a Teflon mold, and further removal of solvent residue in a vacuum oven over two days. The mechanical properties of the elastomeric samples are summarized in Table 1. Note that PDMS is a viscous liquid while bpy-PDMS is a solid due to hydrogen bonding of the amides and π-π interactions between the bipyridine units. Despite the differences in the dynamic properties of crosslinkers, all polymers showed comparable Young's modulus in the elastic region (E: ~1MPa within strain < 10%). The metal-ligand coordination cross-linkage also displayed hydrolytic stability. Neither weight nor mechanical properties of the polymers were affected after being immersed in water overnight.

To further correlate the kinetic stability of the crosslinkers with dynamic properties of the polymer, cyclic stress-strain hysteresis and stress relaxation studies were performed. From the cyclic stress-strain experiments, the functionalized PDMS demonstrated different extent of hysteresis between loading and unloading curves (Fig. 3a). The extent of hysteresis was consistent with the stress relaxation experiments (Fig. 3b) and tensile stress variation with displacement rates (Fig. S6). With Zn^{2+} as the crosslinkers, the polymers exhibited much larger hysteresis and faster stress relaxation rate compared to those with Fe^{2+} as the crosslinkers. The Zn^{2+} crosslinkers' superior ability to dissipate energy upon mechanical stress is owing to two factors: firstly, Zn^{2+}-N(bipyridyl) bond is more kinetically labile than that of Fe^{2+}-N(bipyridyl); secondly, the aptitude of Zn^{2+} ions to adopt both octahedral and tetrahedral geometries offers another avenue to minimize stress concentration. Notably, the stress relaxation rate is also related to the choices of counter anions. The stress relaxation rates found in polymers in the order of $Zn(OTf)_2$-PDMS > $Zn(ClO_4)_2$-PDMS > $ZnCl_2$-PDMS suggest that the degree of polymer dynamics follow the same order. Based on this, we propose that the counter anions with different coordinating abilities might also affect the coordination geometry, which is then closely related to the polymer dynamics. The proposed dynamic coordination geometry under mechanical stress is illustrated in Fig. 1b. After the dissociation of Zn^{2+}–N(bipyridyl) bond, it is likely that the weakly coordinating triflate anions

would temporarily occupy the empty coordination sites to stabilize the polymer network. In contrast, more labile anions ClO_4^- don't have the ability to coordinate, while strongly coordinating anions Cl^- would block the coordination sites and disrupt the polymer network. More detailed investigation of mechanical properties and their correlation to molecular structures is not a focus of this report and will be a subject for future study. Lastly, though the un-crosslinked bpy-PDMS polymer also showed large hysteresis and fast stress relaxation rate, this was more of a phenomenon of thermoplastic deformation from irreversible interchain slipping.

To test the self-healing ability, polymer films were cut through completely with a razor blade and the cut interfaces were gently pushed together for a few seconds, then left to allow self-healing at room temperature (r.t) for two days. The polymers' self-healing efficiency is defined as the fracture strain of healed sample to that of the pristine sample in stress-strain experiments. Fig. 3c shows the strain and stress at break of pristine and healed $Zn(OTf)_2$-PDMS films, with healing efficiency of 76±22%. Notably, the healing efficiencies were not significantly affected by surface aging effects. With the cut surfaces of $Zn(OTf)_2$-PDMS film exposed at ambient condition for 24h, the polymer film still retained a self-healing efficiency of ~60%. Lower healing efficiencies, of 55±21% and 21±3% were observed for $Zn(ClO_4)_2$-PDMS and $ZnCl_2$-PDMS (Fig. 3f). Fe^{2+} crosslinker polymers showed insignificant amount of self-healing ability at r.t due to the kinetically inert Fe^{2+}-N(bipyridyl) coordination at r.t[35]. The trend of polymers' self-healing efficiencies follows the order of the dynamics of coordination geometries on the molecular level, that is, a higher degree of the cross-linker dynamics endows polymers better self-healing ability. Not surprisingly, the Fe^{2+} cross-linked polymers were completely healable upon heating at 90 °C for a few hours, owing to mutual contributions of higher degree of polymer chain mobility and more labile Fe^{2+}-N(bipyridyl) coordination at higher temperature[35]. Furthermore, the un-crosslinked bpy-PDMS polymer displayed minimal self-healing ability at r.t, verifying that the self-healing in the metal ions cross-linked polymers was mainly due to the metal-ligand coordination.

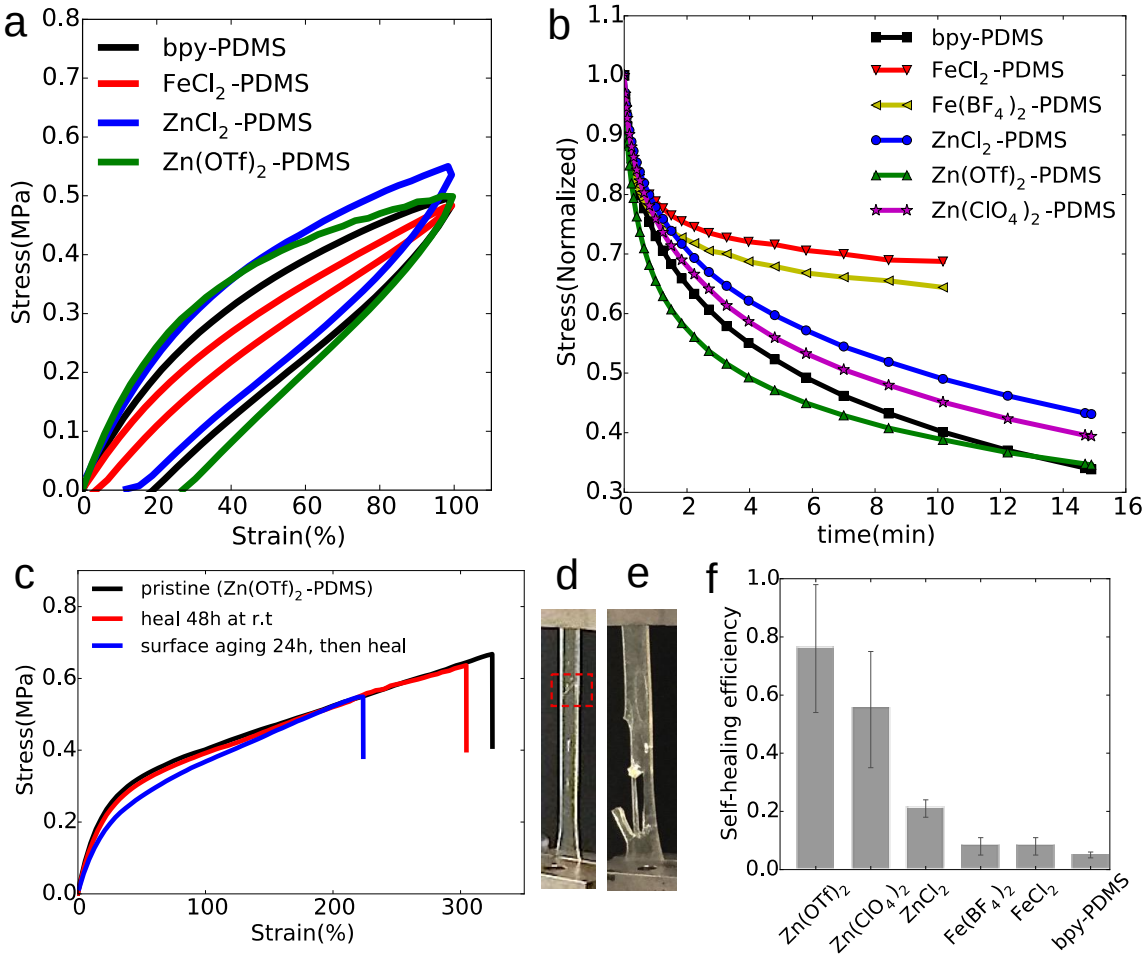

Figure 3 (**a**) The stress-strain curves of polymers bpy-PDMS, $FeCl_2$-PDMS, $ZnCl_2$ and $Zn(OTf)_2$-PDMS, showing different degrees of hysteresis (displacement rate: 5mm/min). (**b**) Stress relaxation data for all polymers. (**c**) Self-healing test for $Zn(OTf)_2$-PDMS polymer at ambient condition without any intervention. (**d**), (**e**) Images showing the self-healed $Zn(OTf)_2$-PDMS polymer film under tensile stress (>250% strain): (**d**) the pristine film was cut into two pieces then subjected to self-heal and the joining edge of the cut films is highlighted in red dot box; (**e**) the pristine film was ruptured into two pieces under tensile stress, the ruptured surface was then gently pushed back together and subjected to self-heal. This image clearly shows parts of the ruptured surface were completely healed to withstand the tensile stress. (**f**) The bar graph summarizing the self-healing efficiencies of all polymers at ambient condition after 48 hrs.

2.3 Electrical Properties

Electrical stability of the transistor elements is crucial in integrated organic circuits[36]. In OFETs, the presence of mobile ions in the dielectric might result in hysteresis effects in the transfer characteristics (I_{DS} vs V_{GS}), indicating an electrical instability[37]. Polymer dielectrics are often hosts for mobile ions, the source of which may potentially come from crosslinking reagents or salt impurities incorporated during material synthesis and handling. The hysteresis due to mobile ionic impurities in OFETs have been observed in poly(vinyl alcohol)[38], fluorinated elastomers[39] and thermoplastic polyurethane gate dielectrics[40]. As metal ions were deliberately added into our materials to serve as cross-linkers, it was imperative to study the presence of ionic effects in the materials as gate dielectrics.

A metal-insulator-metal (MIM) device structure was used for capacitance measurements. The capacitance values of metal ions cross-linked PDMS all demonstrated stability over a wide range of operating frequencies from 20 to 10^5 Hz, as shown in Figure 4. As ionic polarization often occurs at low frequencies, an upper bound on the capacitance was obtained by quasistatic capacitance measurements via the time response of a resistor–capacitor (RC) circuit containing a reference resistor of about 500 MΩ[39]. The capacitance values extracted using this method correspond to a frequency window of 0.05 Hz < f < 1Hz and are similar to the value at much higher frequencies, indicating no ionic effects in dielectric behavior in these polymer system. The low ionic mobility in the functionalized PDMS elastomers is related to both the non-polar siloxane matrix and the stable coordination between bipyridine moieties and the metal salts. The dielectric constants of metal ions cross-linked PDMS are summarized in Table 1. The addition of metal ions has effectively increased the material's dielectric constant compared to the pure bipyridyl-bridged bpy-PDMS. This is desirable as an increase of the dielectric constant of insulating material could lower the operating voltage of transistors.

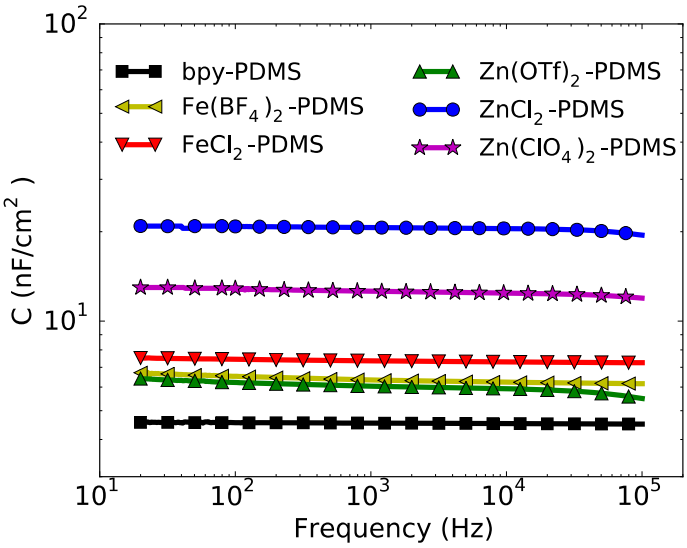

Figure 4 The capacitance versus frequency measured for various functionalized PDMS (bpy-PDMS: 550nm; $Fe(BF_4)_2$-PDMS: 490nm; $FeCl_2$-PDMS: 386nm; $Zn(OTf)_2$-PDMS: 470nm; $ZnCl_2$-PDMS: 138nm; $Zn(ClO_4)_2$-PDMS: 238nm.

To test the feasibility of the metal ions cross-linked PDMS as gate insulators, OFETs were fabricated using either p- or n-type polymeric semiconductor in a bottom-contact top-gate device geometry with the dielectric directly coated onto the semiconductor film (Fig. 5a). The p-type semiconductors used here are a series of previously reported donor-acceptor tetrathienoacene-diketopyrrolopyrrole (TTA-DPP) based polymers (**P1**-**P3**, Fig. 5b) with different side chains and backbone spacers[41], while n-type semiconducting channel layer uses poly(naphthalenediimide-bithiophene)(P(NDI2OD-T2) polymer (**N1**)[42]. The effects of mobile ions in the dielectrics were investigated through the hysteresis from the cyclic transfer characteristics ($\mathbf{I_D}$ vs. $\mathbf{V_G}$) where $\mathbf{I_D}$ depends on the sweep direction of $\mathbf{V_G}$. As shown in Fig. 5c and 5e (Fig. S9, S10 in SI), p-type polymeric semiconductors based OFETs with $FeCl_2$-PDMS or $ZnCl_2$-PDMS dielectric layer all exhibited ideal, hysteresis-free transfer characteristics. In contrast, with $Fe(BF_4)_2$-PDMS, $Zn(ClO_4)_2$-PDMS, or $Zn(OTf)_2$-PDMS dielectrics, the p-type OFETs all demonstrated prominent hysteresis phenomena with a higher back sweep current (the sweep from on to off). This is explained by the mobile anions drifting in the dielectrics when a gate field is applied (Fig. 5i-5k; Fig S11, S12 in SI). Upon applying an "on" gate voltage (negative bias), the anions move towards the dielectric/semiconductor interface. When $\mathbf{V_G}$ is swept back, initially, the anions stay localized at the interface increasing the effective electric field, causing therefore higher back sweep current, i.e. current hysteresis. The hysteresis phenomena also increase with slower gate voltage sweep rate, which is consistent with the explanation that a higher number of mobile anions accumulate close to the dielectric/semiconductor interface when the on-voltage bias is applied for a longer time. It is also apparent that dielectrics with larger-sized counter anions displayed wider hysteresis in the transfer characteristics. With the addition of metal salts as the crosslinkers for the dielectric polymer matrix, the metal cations (Fe^{2+}, Zn^{2+}) are affixed to the polymer backbone via coordination bonds, the counter anions with a smaller size would result in stronger ion pairs, which can inhibit mobile anions drifting under electric bias. This explains the absence of hysteresis in $FeCl_2$-PDMS or $ZnCl_2$-

PDMS dielectrics with the small-sized counter anion Cl^- and also provides important guidance for future dielectric material design.

Similar hysteresis phenomena were also observed in n-type polymeric semiconductors based OFETs. With $Zn(OTf)_2$-PDMS dielectrics (Fig. S12c in SI), the OFETs displayed a higher back sweep current. Upon applying an "on" gate voltage (positive bias), the anions move away from the semiconductor, leaving the positively charged polymer backbone close to the dielectric/semiconductor interface. When V_G is swept back, the positively charged polymer backbone increases the effective gate field and causes higher back sweep current, i.e current hysteresis. With $FeCl_2$-PDMS (Fig. 5g) or $ZnCl_2$-PDMS (Fig. S10d in SI) as dielectrics, the OFETs displayed a lower back sweep current hysteresis dominated by the trapping of charge carriers at the semiconductor-dielectrics interface. With a slower gate voltage sweep rate, the lower back sweep current hysteresis can be eliminated in the case of $FeCl_2$-PDMS dielectrics, suggesting that the electron traps are filled. This further proves the absence of mobile anions drifting in $FeCl_2$-PDMS and $ZnCl_2$-PDMS dielectrics.

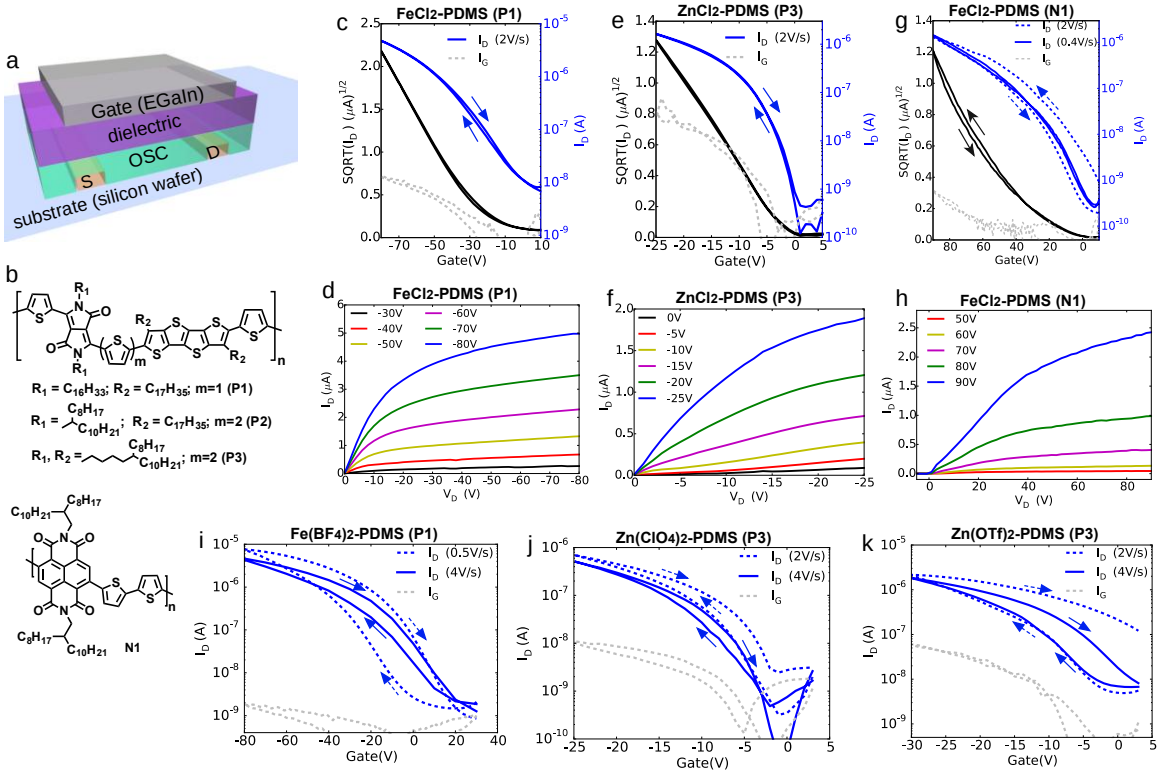

Figure 5 (**a**) Schematic of the organic field-effect transistor (OFET) device structure in a top-gate bottom-contact geometry on rigid substrate (silicon wafer). (**b**) Chemical structures of P-type (**P1-P3**) and N-type (**N1**) organic semiconducting (OSC) polymers used here. (**c-k**) Transfer (I_d versus V_g) and output curve characteristics of OFETs with channel width of 4000 μm (arrows denote gate bias sweep directions and the gate voltage scan rate is normalized to that of 1um thickness): (**c**) Transfer curve and (**d**) output curve of **P1**, with 5.5 μm thick **$FeCl_2$-PDMS** as dielectrics (C: 0.56 nF/cm^2, channel L: 50μm). (**e**) Transfer curve and **(f)** output curve of **P3**, with 1.2μm thick **$ZnCl_2$-PDMS** as dielectrics (C: 2.4 nF/cm^2, channel L: 100μm). (**g**) Transfer curve and (**h**) output curve of **N1**, with 5.5μm thick **$FeCl_2$-PDMS** as dielectrics (C: 0.56 nF/cm^2, channel L: 50 μm) (**i**) Transfer curve of **P1**, with 6 μm thick **$Fe(BF_4)_2$-PDMS** as dielectrics (C: 0.53 nF/cm^2, channel L: 50μm). (**j**) Transfer curve of **P3**, with 1.4 μm thick **$Zn(ClO_4)_2$-PDMS** as dielectrics (C: 2.2nF/cm^2, channel L: 200μm). (**k**) Transfer curve of **P3** with 1.5μm thick **$Zn(OTf)_2$-PDMS** as dielectrics (C: 2.1nF/cm^2, channel L: 200μm).

Encouraged by the stable electrical performance of metal salts crosslinked elastomers containing Cl^- anions, we then fabricated fully stretchable transistors with $FeCl_2$-PDMS as dielectrics and P2 or P3 as p-type polymeric semiconductors. Bottom contact, top gate devices were fabricated using sequential lamination transfers from rigid silicon substrates according to a procedure modified from our previously published work[43]. Briefly, unsorted CNTs were spray coated onto an octadecyltrimethoxysilane(OTMS)-treated wafer[44], then followed by patterning and lamination onto hydrogenated styrene butadiene block copolymer (SEBS) substrates to form source and drain electrodes. Polymeric semiconductors and dielectrics spin-coated on separate OTMS-treated wafers were sequentially transferred onto the SEBS substrate (Fig. 6a). The transistor device was completed via the application of EGaIn liquid metal on top as the gate electrode. Representative transfer curves with P2 or P3 as semiconductors are shown in Fig. 6d-f, which exhibits ideal, hysteresis-free transfer characteristics. Strain dependence of the transistor performance was evaluated by stretching the substrate both parallel and perpendicular to the charge transport direction. Within both tested strain range and directions, the fully stretchable transistors retained good transfer characteristics, suggesting that the semiconductor and dielectrics remain good contact interface when the device is under mechanical deformation. Though the mobility of the transistor decreases under strain, this is intrinsic to the properties of polymeric semiconductors used here, which form cracks under strain and thus exhibit a drop of mobility. Notably, the gate leakage current remains under 1 nA even after 1000 cycles of strain up to 100% (Fig. 6d), indicating the mechanical robustness of the $FeCl_2$-PDMS dielectric film.

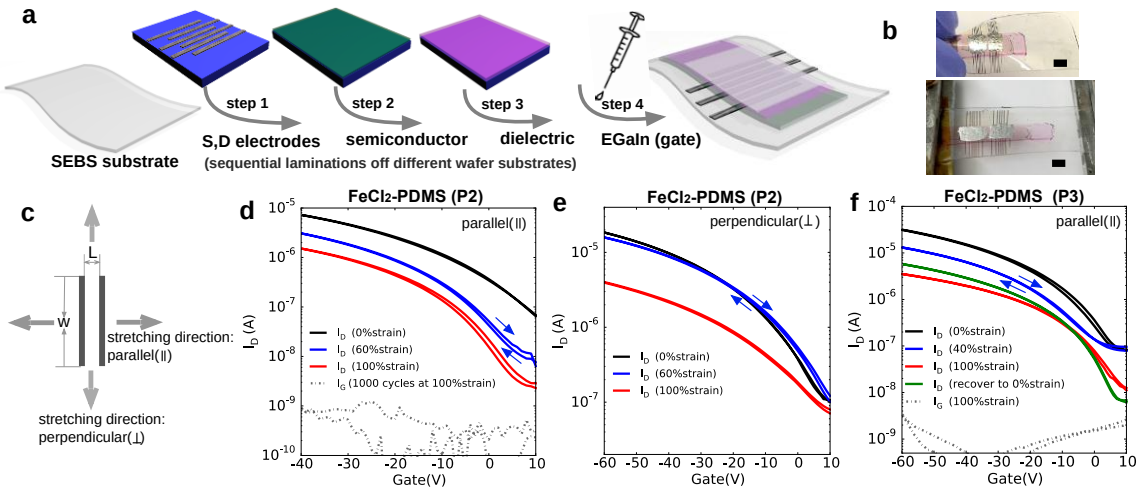

Figure 6 (**a**) Fabrication flow of fully stretchable transistors. (**b**) Images of the flexible device at 0% (top) and 100% (bottom) tensile strain, scale bar: 4mm. (c) Diagram depicting the stretching direction. (**d-f**) Transfer curve (I_d versus V_g) characteristics of fully stretchable transistors of **P2** (**d**, **e**) and **P3** (**f**), with 3.5 μm thick **$FeCl_2$-PDMS** as dielectrics (C: 0.85 nF/cm^2, channel W: 4000μm, L: 50μm) at various tensile strain.

3. Conclusions

In summary, we have demonstrated a new class of metal salts crosslinked elastomers based on the metal-ligand coordination between transition metal ions (Fe^{2+}, Zn^{2+}) and bipyridine moieties incorporated in the PDMS backbone. The identity of metal cations and their counter anions determine the coordination geometry and bond strength, and are used to further influence the bulk polymer's mechanical properties and electrical performances. The polymers' self-healing ability is primarily determined by the kinetic lability of the metal-ligand coordination bonds. We found that PDMS polymers crosslinked with zinc salts ($Zn(OTf)_2$, $Zn(ClO_4)_2$) exhibited much better self-healing abilities than those of polymers crosslinked with iron salts. Moreover, surface aging has minimal effects on self-healing efficiency. Addition of metal salts as polymer crosslinkers also serves as an effective strategy to increase the materials' dielectric constants, while maintaining the stable capacitance without introducing undesirable ionic effects. When the metal salts crosslinked PDMS integrated into OFETs as a dielectric layer, the electrical stability of the transistor is closely related to the ion pair strength of the metal salts. Transistors with $FeCl_2$-PDMS or $ZnCl_2$-PDMS as dielectrics demonstrated ideal, hysteresis-free transfer characteristics, owing to that the strong columbic interaction between metal ion and small Cl^- anion can prevent mobile anions drifting under gate bias. Fully stretchable transistors with $FeCl_2$-PDMS dielectrics also displayed stable transfer characteristics and low gate leakage current after 1000 cycles at 100% strain. The mechanical robustness and stable electrical performance proved that metal salts crosslinked non-polar PDMS are suitable for applications in stretchable electronics, for potential applications in wearable sensors and electronic skins. Similar coordination chemistry could be potentially expanded into other polymer matrices to allow additional tunabilities. We conclude that to obtain polymer dielectrics possessing both autonomous self-healing ability and stable electrical performances, utilizing high coordinate metal ion which can form flexible, labile coordination geometry with ligands, and strong interaction with the counter anions is a desirable strategy.

Table 1 Summary of mechanical properties and dielectric constants of polymers.

Polymer	E(MPa)[a]	ε (%)[b]	ε_r[c]
bpy-PDMS	1.0±0.1	87±15	2.9
$FeCl_2$-PDMS	0.9±0.2	125±20	3.5
$Fe(BF_4)_2$-PDMS	1.0±0.15	110±16	3.6
$ZnCl_2$-PDMS	1.2±0.21	143±20	3.3
$Zn(ClO_4)_2$-PDMS	1.2±0.15	295±17	3.5
$Zn(OTf)_2$-PDMS	1.1±0.2	310±15	3.5

[a] Young's modulus, calculated from the initial slope of stress-strain curves (within 10% strain). [b] ultimate tensile strain (displacement rate: 5mm/min). [c] dielectric constant.

Table 2 Summary of OFETs electrical performances of various semiconductors (**P1**, **P2**, **P3** and **N1**), using $FeCl_2$-PDMS or $ZnCl_2$-PDMS as dielectrics (channel W: 4000 μm; L: 50 μm).

OSC	$FeCl_2$-PDMS					$ZnCl_2$-PDMS				
	d[1] (μm)	C[2] (nF/cm^2)	μ (cm^2/V·s)	V_{th}	on/off	d (μm)	C (nF/cm^2)	μ (cm^2/V·s)	V_{th}	on/off
P1	3.5	0.88	0.19±0.03	-15±2	5.9×10^3	5	0.58	0.17±0.03	-21±4	3.2×10^3
	5.5	0.56	0.16±0.02	-18±4	2.1×10^3					
P2	3.5	0.88	0.18±0.02	7±3	4.4×10^3	3	0.97	0.2±0.02	1.1±0.6	2.1×10^3
P3	3.5	0.88	0.35±0.1	2.5±5	1.3×10^3	1.2	2.4	0.29±0.06	-2±2	1.2×10^4
N1	5.5	0.56	0.11±0.04	27±10	5.3×10^3	1.2	2.4	0.14±0.03	1.2±5	2.7×10^3

[1] Dielectric thickness. [2] The dielectric capacitance value.

Acknowledgements

This work was supported by Samsung Electronics. Y-L. R. thanks the Canadian Natural Science and Engineering Research Council (NSERC) Postdoctoral Fellowship. R.P. is grateful to Generalitat de Catalunya for a Beatriu de Pinós, Marie Curie COFUND fellowship.

Supporting information

Synthesis, UV-Vis absorption titration, TGA, DSC, mechanical test, device fabrications, additional transistors transfer characteristics, SAXS data. This material is available free of charge via the Internet at http://pubs.acs.org.

Competing financial interests

The authors declare no competing financial interests.

References

(1) Rogers, J. A.; Someya, T.; Huang, Y. *Science* **2010**, *327*, 1603.

(2) Park, S.; Vosguerichian, M.; Bao, Z. *Nanoscale* **2013**, *5*, 1727.

(3) Sekitani, T.; Someya, T. *Adv. Mater.* **2010**, *22*, 2228.

(4) Ko, H.; Kapadia, R.; Takei, K.; Takahashi, T.; Zhang, X.; Javey, A. *Nanotechnology* **2012**, *23*, 344001.

(5) Kim, D.-H.; Ghaffari, R.; Lu, N.; Rogers, J. A. *Annu. Rev. Biomed. Eng.* **2012**, *14*, 113.

(6) Arias, A. C.; MacKenzie, J. D.; McCulloch, I.; Rivnay, J.; Salleo, A. *Chem. Rev.* **2010**, *110*, 3.

(7) Irimia-Vladu, M.; Głowacki, E. D.; Voss, G.; Bauer, S.; Sariciftci, N. S. *Mater. Today* **2012**, *15*, 340.

(8) Bettinger, C. J.; Bao, Z. *Adv. Mater.* **2010**, *22*, 651.

(9) Hammock, M. L.; Chortos, A.; Tee, B. C. K.; Tok, J. B. H.; Bao, Z. *Adv. Mater.* **2013**, *25*, 5997.

(10) Rivnay, J.; Owens, R. M.; Malliaras, G. G. *Chem. Mater.* **2014**, *26*, 679.

(11) Tee, B. C.-K.; Wang, C.; Allen, R.; Bao, Z. *Nat. Nanotechnol.* **2012**, *7*, 825.

(12) Chen, P.; Li, Q.; Grindy, S.; Holten-Andersen, N. *J. Am. Chem. Soc.* **2015**, *137*, 11590.

(13) Wang, C.; Wu, H.; Chen, Z.; McDowell, M. T.; Cui, Y.; Bao, Z. *Nat. Chem.* **2013**, *5*, 1042.

(14) Yang, Y.; Urban, M. W. *Chem. Soc. Rev.* **2013**, *42*, 7446.

(15) Williams, K. A.; Boydston, A. J.; Bielawski, C. W. *J. R. Soc. Interface* **2007**, *4*, 359.

(16) Burnworth, M.; Tang, L.; Kumpfer, J. R.; Duncan, A. J.; Beyer, F. L.; Fiore, G. L.; Rowan, S. J.; Weder, C. *Nature* **2011**, *472*, 334.

(17) Holten-Andersen, N.; Harrington, M. J.; Birkedal, H.; Lee, B. P.; Messersmith, P. B.; Lee, K. Y. C.; Waite, J. H. *Proc. Natl. Acad. Sci. U. S. A.* **2011**, *108*, 2651.

(18) Mozhdehi, D.; Ayala, S.; Cromwell, O. R.; Guan, Z. *J. Am. Chem. Soc.* **2014**, *136*, 16128.

(19) Li, C-H.; Wang, C.; Keplinger, C.; Zuo, J-L.; Jin, L.; Sun, Y.; Zheng, P.; Cao, Y.; Lissel, F.; Linder, C.; You, X-Z.; Bao, Z. *Nat. Chem*. DOI: 10.1038/NCHEM.2492.

(20) Lu, C.-C.; Lin, Y.-C.; Yeh, C.-H.; Huang, J.-C.; Chiu, P.-W. *ACS Nano* **2012**, *6*, 4469.

(21) Huang, W.; Besar, K.; Zhang, Y.; Yang, S.; Wiedman, G.; Liu, Y.; Guo, W.; Song, J.; Hemker, K.; Hristova, K.; Kymissis, I. J.; Katz, H. E. *Adv. Funct. Mater.* **2015**, *24*, 3745.

(22) Kaes, C.; Katz, A.; Hosseini, M. W. *Chem. Rev.* **2000**, *100*, 3553.

(23) Ayme, J.-F.; Beves, J. E.; Campbell, C. J.; Gil-Ramírez, G.; Leigh, D. a.; Stephens, A. J. *J. Am. Chem. Soc.* **2015**, *137*, 9812.

(24) Guo, J.; Mayers, P. C.; Breault, G. A.; Hunter, C. A. *Nat Chem* **2010**, *2*, 218.

(25) Ye, B. H.; Tong, M. L.; Chen, X. M. *Coord. Chem. Rev.* **2005**, *249*, 545.

(26) Przybyla, D. E.; Chmielewski, J. *J. Am. Chem. Soc.* **2008**, *130*, 12610.

(27) Przybyla, D. E.; Chmielewski, J. *J. Am. Chem. Soc.* **2010**, *132*, 7866.

(28) Decurtins, S.; Schmalle, H. W.; Schneuwly, P.; Oswald, H. R. *Inorg. Chem.* **1993**, *32*, 1888.

(29) Sénéchal, K.; Maury, O.; Le Bozec, H.; Ledoux, I.; Zyss, J. *J. Am. Chem. Soc.* **2002**, *124*, 4560.

(30) Younes, A. H.; Zhang, L.; Clark, R. J.; Zhu, L. *J. Org. Chem.* **2009**, *74*, 8761.

(31) Chen, X. M.; Wang, R. Q.; Yu, X. L. *Acta Crystallogr. Sect. C Cryst. Struct. Commun.* **1995**, *51*, 1545.

(32) Kean, Z. S.; Hawk, J. L.; Lin, S.; Zhao, X.; Sijbesma, R. P.; Craig, S. L. *Adv. Mater.* **2014**, *26*, 6013.

(33) Shankar, S.; Lahav, M.; van der Boom, M. E. *J. Am. Chem. Soc.* **2015**, *137*, 4050.

(34) Khan, M. A.; Tuck, D. G. *Acta Crystallogr., Sect. C Cryst. Struct. Commun.* **1984**, *40*, 60.

(35) Akhuli, B.; Cera, L.; Jana, B.; Saha, S.; Schalley, C. a; Ghosh, P. *Inorg. Chem.* **2015**, *54*, 4231.

(36) Facchetti, A.; Yoon, M.-H.; Marks, T. J. *Adv. Mater.* **2005**, *17*, 1705.

(37) Egginger, M.; Bauer, S.; Schwödiauer, R.; Neugebauer, H.; Sariciftci, N. S. *Monatshefte fur Chemie* **2009**, *140*, 735.

(38) Egginger, M.; Irimia-Vladu, M.; Schwödiauer, R.; Tanda, a.; Frischauf, I.; Bauer, S.; Sariciftci, N. S. *Adv. Mater.* **2008**, *20*, 1018.

(39) Wang, C.; Lee, W.-Y.; Kong, D.; Pfattner, R.; Schweicher, G.; Nakajima, R.; Lu, C.; Mei, J.; Lee, T. H.; Wu, H.-C.; Lopez, J.; Diao, Y.; Gu, X.; Himmelberger, S.; Niu, W.; Matthews, J. R.; He, M.; Salleo, A.; Nishi, Y.; Bao, Z. *Sci. Rep.* **2015**, *5*, 17849.

(40) Chortos, A.; Koleilat, G. I.; Pfattner, R.; Kong, D.; Lin, P.; Nur, R.; Lei, T.; Wang, H.; Liu, N.; Lai, Y.-C.; Kim, M.-G.; Chung, J. W.; Lee, S.; Bao, Z. *Adv. Mater.* **2015**, DOI: 10.1002/adma.201501828.

(41) Matthews, J. R.; Niu, W.; Tandia, A.; Wallace, A. L.; Hu, J.; Lee, W. Y.; Giri, G.; Mannsfeld, S. C. B.; Xie, Y.; Cai, S.; Fong, H. H.; Bao, Z.; He, M. *Chem. Mater.* **2013**, *25*, 782.

(42) (a) Yan, H.; Chen, Z.; Zheng, Y.; Newman, C.; Quinn, J. R.; Dötz, F.; Kastler, M.; Facchetti, A. *Nature*. **2009**, *457*, 679. (b) Kurosawa, T.; Chiu, Y.-C.; Zhou, Y.; Gu, X.; Chen, W.-C.; Bao, Z. *Adv. Funct. Mater.* **2016**, *26*, 1261.

(43) Chortos, A.; Lim, J.; To, J. W. F.; Vosgueritchian, M.; Dusseault, T. J.; Kim, T. H.; Hwang, S.; Bao, Z. *Adv. Mater.* **2014**, *26*, 4253.

(44) Ito, Y.; Virkar, A. A.; Mannsfeld, S.; Oh, J. H.; Toney, M.; Locklin, J.; Bao, Z. *J. Am. Chem. Soc.* **2009**, *131*, 9396.

For Table of Contents (TOC) Only